nature medicine

SUPPLEMENTARY INFORMATION

https://doi.org/10.1038/s41591-018-0032-8

In the format provided by the authors and unedited.

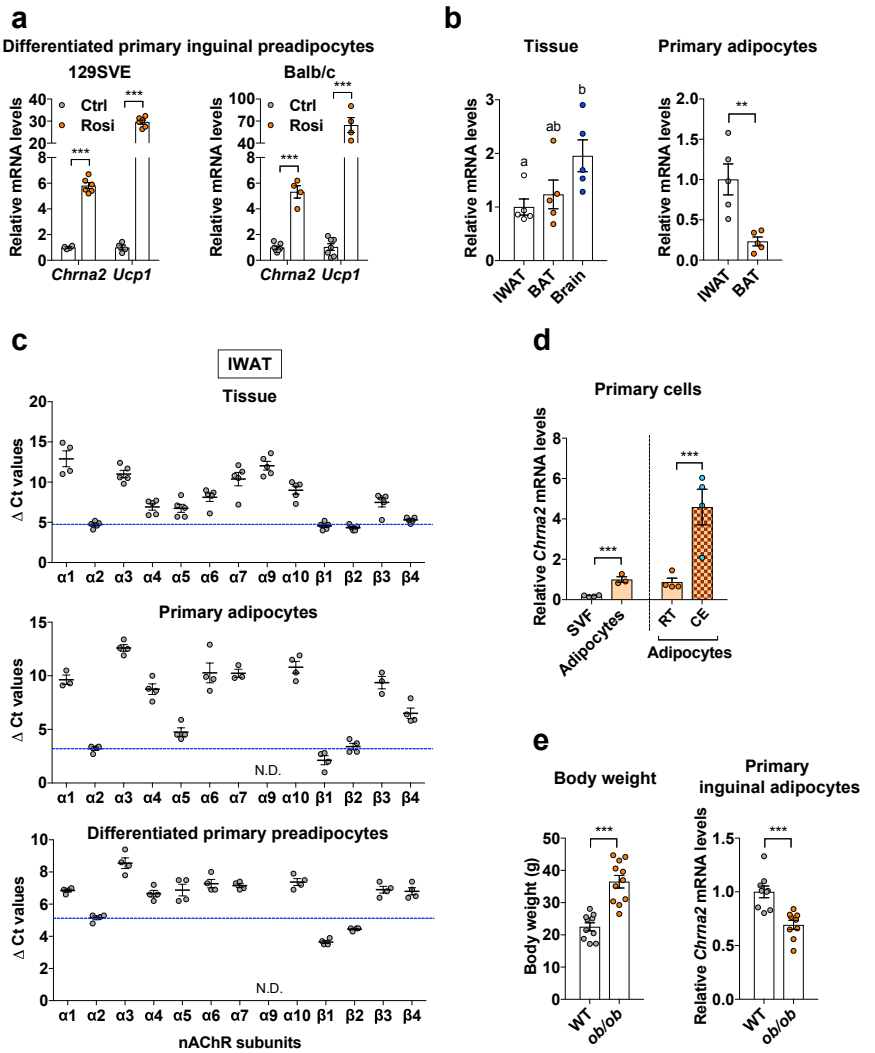
An immune-beige adipocyte communication via nicotinic acetylcholine receptor signaling

Heejin Jun[1], Hui Yu[1,2], Jianke Gong[1,3], Juan Jiang[1,4], Xiaona Qiao[1,5], Eric Perkey[6,7,8], Dong-il Kim[1], Margo P. Emont[1,2], Alexander G. Zestos[9,13], Jung-Sun Cho[1], Jianfeng Liu[3], Robert T. Kennedy[9,10], Ivan Maillard[1,7,11,12,14], X. Z. Shawn Xu[1,2] and Jun Wu[1,2]*

[1]Life Sciences Institute, University of Michigan, Ann Arbor, MI, USA. [2]Department of Molecular and Integrative Physiology, University of Michigan Medical School, Ann Arbor, MI, USA. [3]International Research Center for Sensory Biology and Technology of MOST, Key Laboratory of Molecular Biophysics of MOE, College of Life Science and Technology, Huazhong University of Science and Technology, Wuhan, China. [4]Department of Respiratory Medicine, Key Site of National Clinical Research Center for Respiratory Diseases, Xiangya Hospital, Central South University, Changsha, China. [5]Huashan Hospital, Fudan University, Shanghai, China. [6]Center for Stem Cell Biology, Life Sciences Institute, University of Michigan, Ann Arbor, MI, USA. [7]Graduate Program in Cellular and Molecular Biology, University of Michigan, Ann Arbor, MI, USA. [8]Medical Scientist Training Program, University of Michigan, Ann Arbor, MI, USA. [9]Department of Chemistry, University of Michigan, Ann Arbor, MI, USA. [10]Department of Pharmacology, University of Michigan, Ann Arbor, MI, USA. [11]Division of Hematology–Oncology, Department of Medicine, University of Michigan, Ann Arbor, MI, USA. [12]Department of Cell and Developmental Biology, University of Michigan, Ann Arbor, MI, USA. [13]Present address: Department of Chemistry, Center for Behavioral Neuroscience, American University, Washington, D.C., USA. [14]Present address: Division of Hematology–Oncology, Department of Medicine and Abramson Family Cancer Research Institute, University of Pennsylvania Perelman School of Medicine, Philadelphia, PA, USA. *e-mail: wujunz@umich.edu

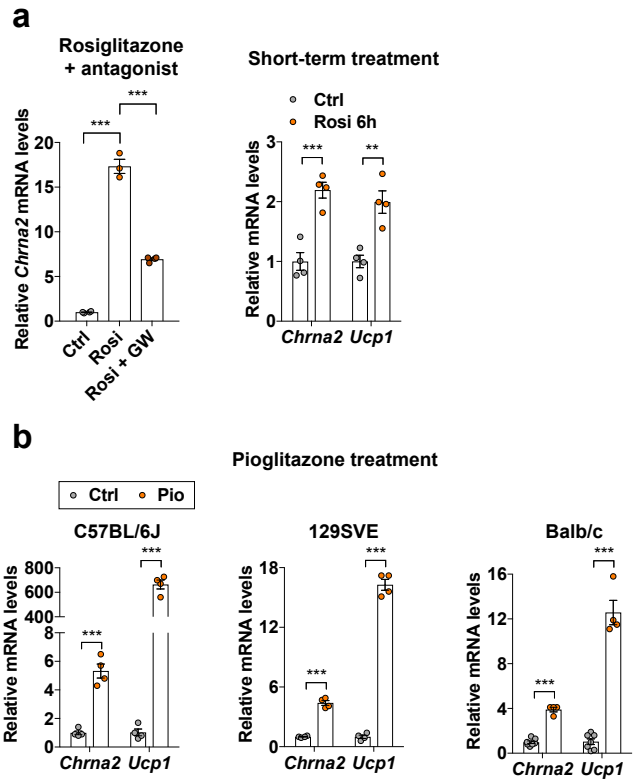
© 2018 Nature America Inc., part of Springer Nature. All rights reserved.

Jun et al.
Supplementary Fig. 1, Related to Fig. 1



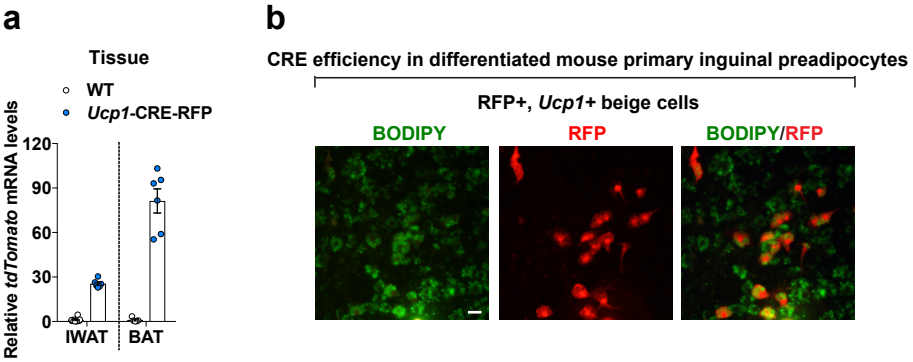
Supplementary Figure 1. *Chrna2* expression. (**a**) *Chrna2* is induced in subcutaneous adipocytes of multiple inbred wild type mouse strains during beiging. qPCR analyses of *Chrna2* and *Ucp1* mRNA expression in differentiated inguinal preadipocytes of 129SVE (n=4 for Ctrl, 6 for Rosi) and Balb/c (n=7 for Ctrl, 4 for Rosi) mice treated with vehicle (Ctrl) or 1μM rosiglitazone (Rosi) for 4 d. (**b**) *Chrna2* is expressed in murine subcutaneous adipocytes. qPCR analyses of *Chrna2* mRNA levels in tissues, IWAT, interscapular BAT, and the brain as a positive control, and primary inguinal and brown adipocytes from C57BL/6J mice (n=5 per group). Interestingly, whereas the α2 subunit expression levels were comparable between IWAT and interscapular BAT, higher expression of the α2 subunit was detected in the fractionated mature adipocytes from IWAT than those from BAT. (**c**) The α2 subunit is expressed at significant levels among nAChR subunits in mouse subcutaneous fat tissue and adipocytes. To date, twelve distinct genes encoding neuronal nicotinic acetylcholine receptor (nAChR) subunits have been identified, nine α-type (α2-α10), and three β-type (β2-β4), generating a large set of structurally and functionally distinct hetero- and homo- pentameric receptors. Some of the other nAChR subunits are detectable in inguinal fat tissue and cultures along with α2, including β1 and β2 . α1 and β1 are muscle-type nAChR subunits. α8 is not listed in the figures since it has only been detected in chicken. qPCR analyses of nAChR subunit mRNA in IWAT (n=5), primary inguinal adipocytes (n=4) and differentiated primary inguinal preadipocytes (n=4) of C57BL/6J mice. The ΔCt value was determined by subtracting the Ct value of reference gene *Tbp* from that of target gene for each sample. A low ΔCt value means high mRNA level. (**d**) *Chrna2* expression is regulated in mature adipocytes of mouse subcutaneous fat in response to cold. qPCR analyses of *Chrna2* mRNA expression in the stromal vascular fraction (SVF, n=4) and mature adipocytes (n=3) fractionated from IWAT of C57BL/6J mice housed at room temperature (RT) or 10ºC for 2 d (CE) (n=4 per group). (**e**) *Chrna2* expression is diminished in subcutaneous adipocytes of obese mice. Body weights of WT (n=10) and *ob/ob* (n=11) mice (left). qPCR analyses of *Chrna2* mRNA expression in mature adipocytes fractionated from IWAT (n=9 per group) of WT and *ob/ob* mice (right). Data are presented as mean ± s.e.m. A different letter denotes a significant difference among groups at $p<0.05$. **$p<0.01$. ***$p<0.001$. N.D., not detectable.

Jun et al.
Supplementary Fig. 2, Related to Fig. 1



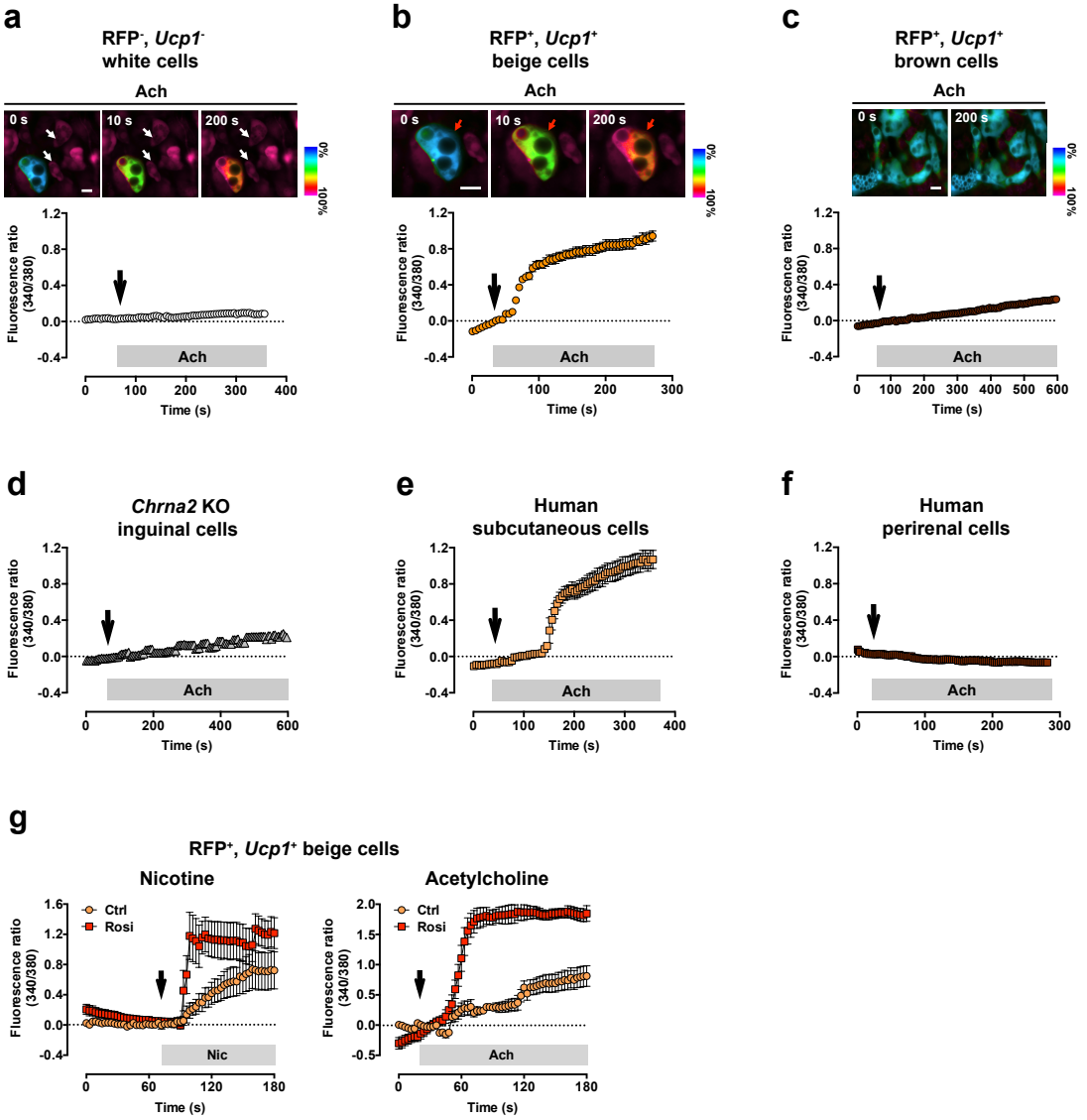
Supplementary Figure 2. Regulation of *Chrna2* expression. (**a**) qPCR analyses of *Chrna2* mRNA levels in differentiated WT inguinal preadipocytes treated with vehicle (Ctrl, n=4), 1 μM rosiglitazone (Rosi, n=3) alone for 2 d or preincubated with 25 μM GW9662 (GW, n=4) for 2 d and then Rosi for 2 d (left). qPCR analyses of *Chrna2* and *Ucp1* mRNA levels in differentiated WT (C57BL/6J) inguinal preadipocytes with treatment of vehicle or 1 μM Rosi for 6 h (n=4 per group) (right). *Chrna2* transcription is directly regulated by PPARγ in mouse subcutaneous adipocytes. Rosi-induced *Chrna2* expression was blunted by co-treatment with the PPARγ antagonist GW (left). Furthermore, *Chrna2* expression was also upregulated by acute treatment with Rosi (6 h) (right), indicating that this induction could be achieved through the direct effects of Rosi. (**b**) qPCR analyses of *Chrna2* and *Ucp1* mRNA expression in differentiated inguinal preadipocytes of C57BL/6J (n=4 per group), 129SVE (n=4 per group) and Balb/c mice (n=6 for Ctrl, 4 for Pio) exposed to vehicle (Ctrl) or 1 μM pioglitazone (Pio) for 4 d. *Chrna2* expression is upregulated in subcutaneous adipocytes of multiple inbred wild type mouse strains in response to the PPARγ agonist Pio. The fact that Pio, another TZD besides Rosi, upregulates *Chrna2* indicates that activated PPARγ directly influences the transcription of *Chrna2*. Data are presented as mean ± s.e.m. ***p*<0.01. ****p*<0.001.

Jun et al.
Supplementary Fig. 3, Related to Fig. 2



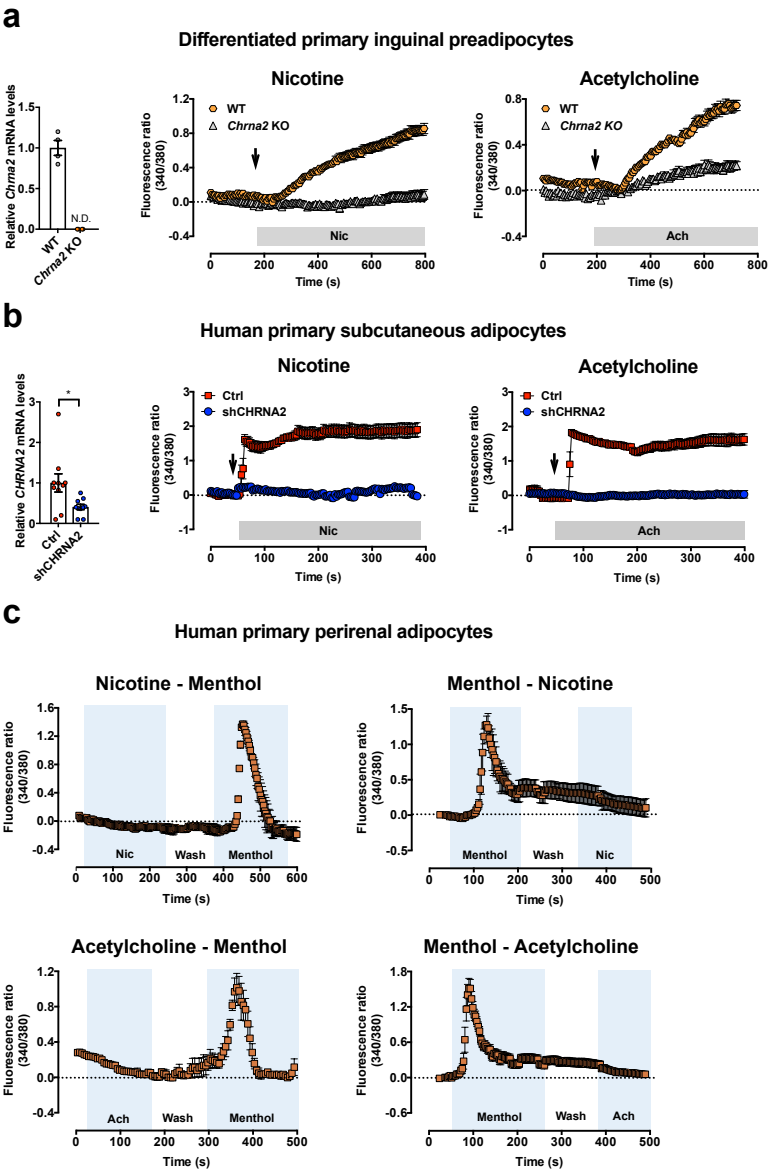
Supplementary Figure 3. *Ucp1*-expressing beige cells are present in differentiated mouse primary inguinal preadipocytes. (**a**) qPCR analyses of *tdTomato* (*Rfp*) mRNA expression in IWAT (n=10 for WT, 6 for *Ucp1*-CRE-RFP) and BAT (n=5 for WT, 6 for *Ucp1*-CRE-RFP) of C57BL/6J (WT, negative control) and *Ucp1*-CRE-RFP mice. (**b**) Beige adipocytes labeled with RFP (red), visible at 550 nm, in differentiated inguinal preadipocytes of *Ucp1*-CRE-RFP mice where lipid droplets are stained with BODIPY (green). Scale bar, 20 μm.

Jun et al.
Supplementary Fig. 4, Related to Fig. 2



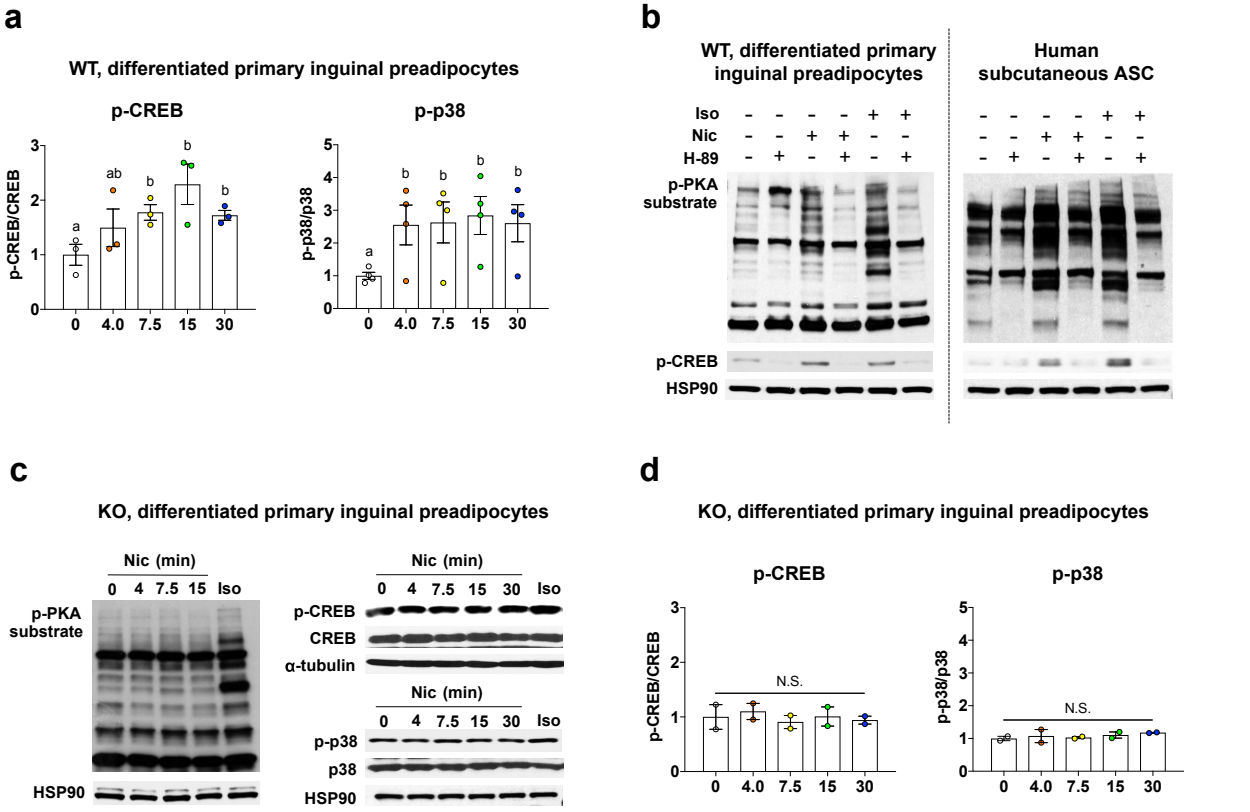
Supplementary Figure 4. CHRNA2 signaling is beige adipocyte-selective. (**a,b**) Intracellular Ca^{2+} rises in response to the CHRNA2 agonist acetylcholine (Ach, 100 μM) only in RFP+ beige adipocytes (red arrow, n=8) (**b**) but not in white adipocytes (white arrow, n=7) (**a**) within the subcutaneous fat culture. Representative images are shown in a pseudo color scale at different time points (0, 10 and 200 s). (**c**) Brown adipocytes of *Ucp1*-CRE-RFP mice do not respond to Ach stimulation (n=8). (**d**) Calcium uptake in response to Ach is absent in the differentiated inguinal SVF from *Chrna2* KO mice (n=17). (**e,f**) Differentiated human adipose stromal cells (ASC) isolated from subcutaneous fat depots (n=4) (**e**) but not those from the perirenal depot (n=13) (**f**), mediate calcium uptake upon Ach stimulation. (**g**) CHRNA2 agonist-induced calcium uptake is increased by rosiglitazone (Rosi) treatment in the *Ucp1*-expressing beige cells. Ca^{2+} uptake in RFP+ beige adipocytes within the subcutaneous fat cultures stimulated with or without 1 μM Rosi for 4 d in response to the CHRNA2 agonist nicotine (Nic, 500 μM, n=7 per group) or Ach (100 μM, n=10 for Ctrl, 7 for Rosi). Intracellular Ca^{2+} was monitored in individual RFP+ beige adipocytes by Fura 2-AM. Cell fate mapping experiments have revealed that, in addition to the interscapular depot where the majority of classical brown adipocytes are located, thermogenic fat cells in the murine perirenal depot also arise from the *Myf5*+ lineage. Analyses of expression levels of previously reported cell type identity markers suggested that UCP1+ fat cells are also present within the human perirenal depot and that these cells are less likely to resemble murine beige adipocytes but are more similar to mouse classical brown fat cells. Scale bar, 10 μm. Data are presented as mean ± s.e.m. At some data points, the error bars are almost invisible.

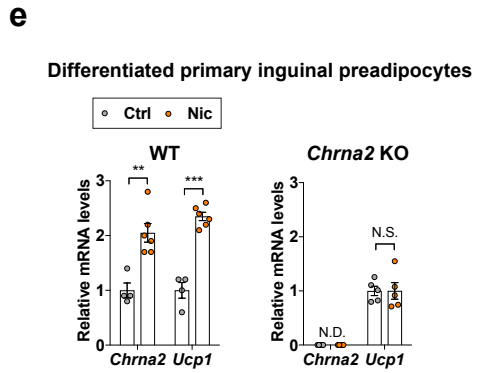
Jun et al.
Supplementary Fig. 5, Related to Fig. 2



Supplementary Figure 5. CHRNA2-dependent calcium uptake in adipocytes. (**a**) Side-by-side comparison of Ca^{2+} uptake in differentiated primary inguinal preadipocytes from WT and *Chrna2* KO mice. Cells which uptake Ca^{2+} in respond to CHRNA2 agonists are present in adipose culture of WT mice, whereas not in those of *Chrna2* KO mice. qPCR analyses of *Chrna2* mRNA expression (left) and calcium uptake analysis in response to CHRNA2 agonists (right) in differentiated primary inguinal preadipocytes of WT and *Chrna2* KO mice (n=4 per group) (**b**) CHRNA2 agonist-induced calcium uptake is blocked by *CHRNA2* knockdown in human subcutaneous adipocytes. qPCR analyses of *Chrna2* mRNA expression in differentiated human subcutaneous adipose precursors transduced with adenoviral control (Ctrl) or shCHRNA2 (n=10 per group) (left). Ca^{2+} uptake in control (Ctrl) and *CHRNA2* knockdown (shCHRNA2) cells in response to the CHRNA2 agonist nicotine (Nic, 500 μM, n=8 for Ctrl, 9 for shCHRNA2) or acetylcholine (Ach, 100 μM, n=8 for Ctrl, 9 for shCHRNA2) (right). Differentiated human subcutaneous adipose precursors were transduced with adenoviral Ctrl or shCHRNA2. High efficiency of virus infection that exceeded 90% was verified at 72 h by the number of GFP-positive cells in both Ctrl and shCHRNA2 groups under fluorescence microscopy. (**c**) Functionally active human perirenal adipocytes are nonresponsive to CHRNA2 agonists. Ca^{2+} uptake in differentiated human adipose stromal cells (ASC) isolated from the perirenal depot in the presence of mammalian cold sensor TRPM8 agonist menthol (300 μM) or CHRNA2 agonist nicotine (Nic, 500 μM) and acetylcholine (100 μM). Menthol-responsive perirenal cells do not respond to nicotine and acetylcholine: Increase in intracellular Ca^{2+} is shown upon menthol stimulation, whereas Ca^{2+} uptake in response to nicotine (n=2 for left and right panels) or acetylcholine (n=2 for left, 3 for right panel) is absent in the differentiated human perirenal ASC. Clean buffer was perfused between two agonists to remove residual agonist that could affect Ca^{2+} uptake of next agonist (wash). Data are presented as mean ± s.e.m. In some mean values, error bars are almost invisible. *p<0.05. N.D., not detectable.

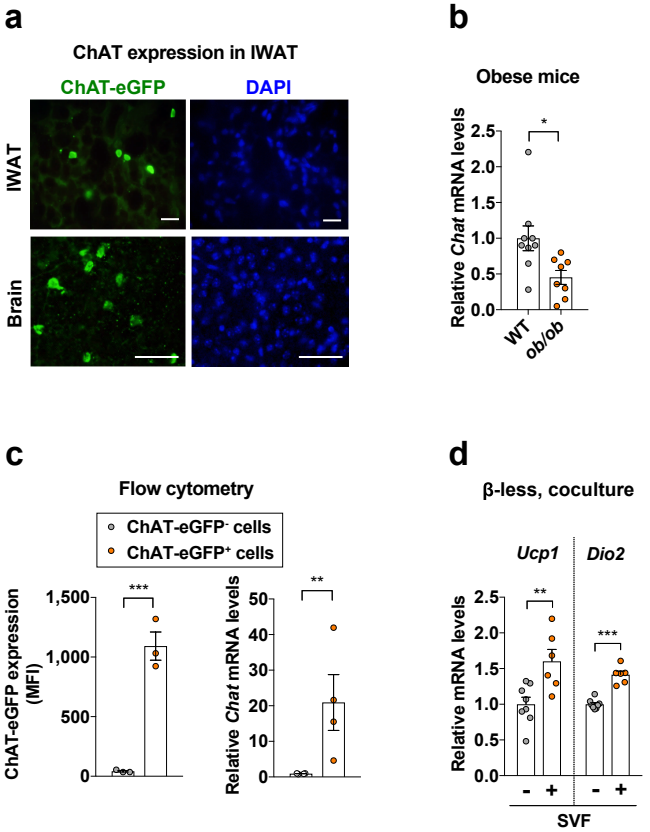
Jun et al.
Supplementary Fig. 6, Related to Fig. 2





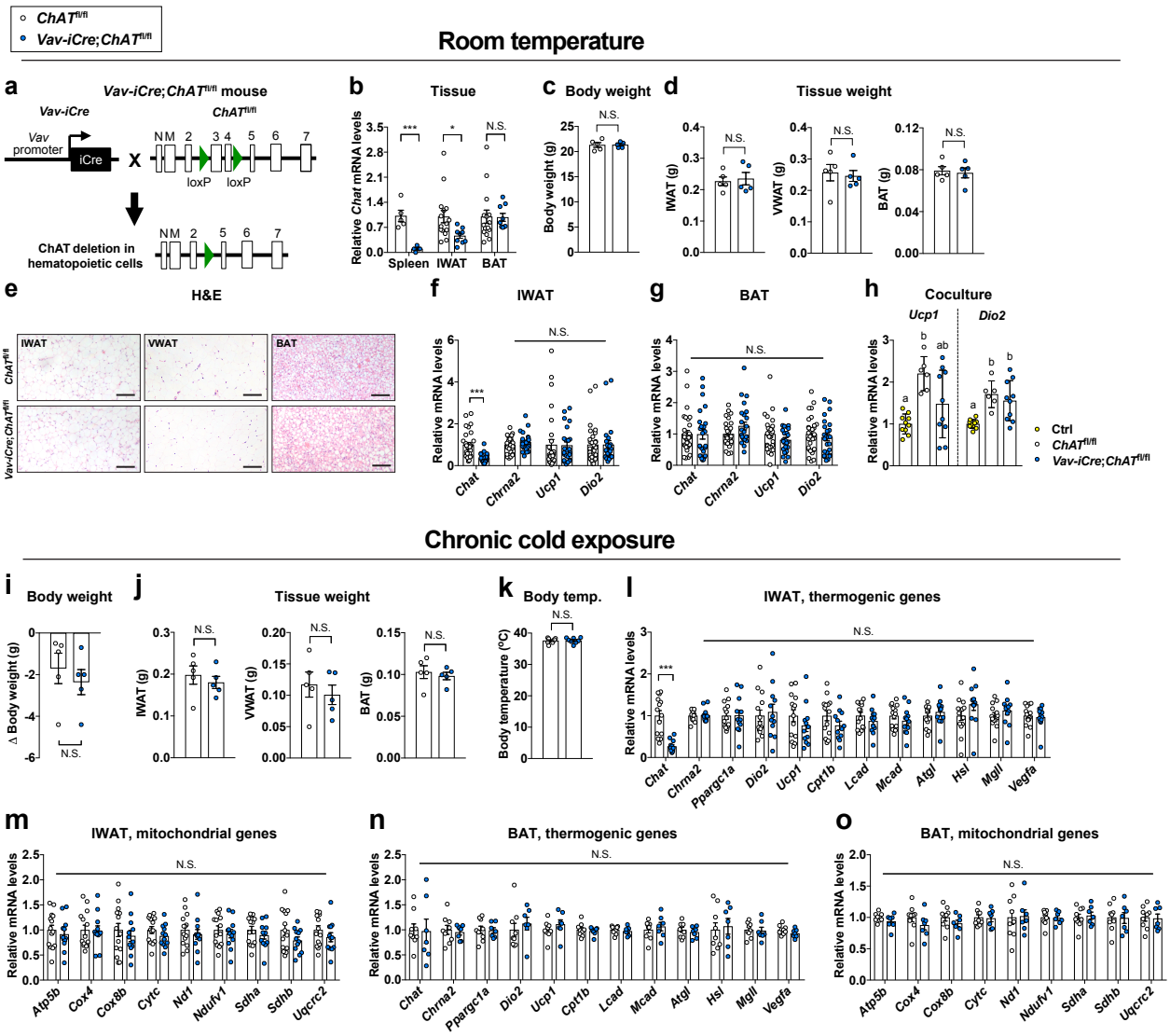
Supplementary Figure 6. CHRNA2 signaling is mediated through PKA in mouse and human subcutaneous adipocytes. (**a**) Quantification of phosphorylated CREB (n=3 per group) and p38 (n=4 per group) proteins in differentiated inguinal preadipocytes of WT mice treated with 2 mM nicotine (Nic) for indicated time assessed by immunoblotting. Representative mmunoblots are shown in Fig. 2i. (**b**) Immunoblots for PKA substrate and CREB phosphorylation in differentiated inguinal preadipocytes of WT mice treated with 50 μM H-89 for 30 min and then 2 mM Nic for 15 min or 10 μM isoproterenol (Iso) for 5 min (left). Immunoblots for phospho-PKA substrate and phospho-CREB in differentiated hASC incubated with 50 μM H-89 for 30 min and then 2 mM Nic or 10 μM Iso for 1 hr (right). (**c**, **d**) The activation of PKA pathway by Nic is CHRNA2-dependent in mouse subcutaneous adipocytes. Immunoblots (**c**) and quantification (**d**) of phosphorylated PKA substrate, CREB and p38 in differentiated inguinal preadipocytes of *Chrna2* KO mice exposed to 2 mM Nic for the indicated time or 10 μM Iso for 5 min as a positive control (n=2 per group for quantification of p-CREB and p-p38). (**e**) *Ucp1* induction is absent in *Chrna2* KO subcutaneous adipocytes upon stimulation with Nic. qPCR analyses of *Chrna2* and *Ucp1* mRNA expression in differentiated primary inguinal preadipocytes of WT (n=4 for Ctrl, 6 for Nic) and *Chrna2* KO (n=5 per group) mice following treatment with vehicle (Ctrl) or 2 mM Nic for 2 d. Data are presented as mean ± s.e.m. $^{**}p<0.01$, $^{***}p<0.001$. A different letter denotes a significant difference among groups at $p<0.05$. N.S., not significant. N.D., not detectable.

Jun et al.
Supplementary Fig. 7, Related to Fig. 3



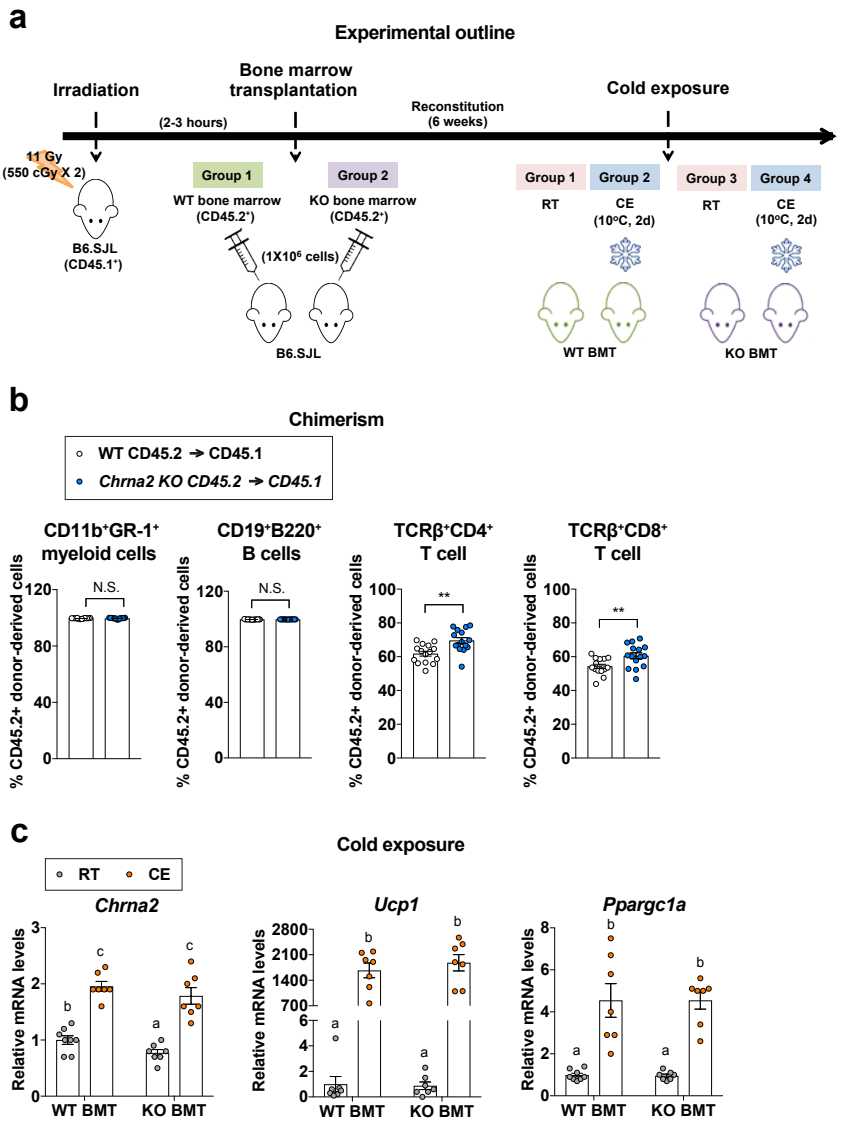
Supplementary Figure 7. *Chat* expression. (**a**) Immunofluorescent staining of GFP in IWAT and brain sections from ChAT^{BAC}-eGFP mice. The brain is included as a positive control where cholinergic neurons are known to be expressing ChAT. Scale bar, 20 μm for IWAT, 50 μm for the brain. (**b**) *Chat* expression is lower in the inguinal stromal vascular fraction (SVF) of obese mice. qPCR analyses of *Chat* mRNA expression in SVF fractionated from IWAT (n=9 for WT, 8 for *ob/ob*). (**c**) ChAT-expressing cells reside in the stromal vascular fraction (SVF) of inguinal adipose tissue. ChAT^{BAC}-eGFP mice provide a convenient model that allows fluorescent visualization of cholinergic elements within both the nervous system and non-neuronal cells. The median fluorescence intensities (MFI) of ChAT-eGFP in the GFP- and GFP+ population of inguinal SVF separated by FACS analyses (n=3 per group) (left). qPCR analyses of *Chat* mRNA levels in GFP- and GFP+ cells of inguinal SVF collected by FACS (n=4 per group) (right). (**d**) qPCR analyses of thermogenic gene expression in differentiated β-less (all three β-adrenergic receptors are knocked out) inguinal preadipocytes cocultured with (n=6) or without (n=8) freshly isolated inguinal SVF from WT mice for 4 h using a two-chamber coculture system. Data are presented as mean ± s.e.m. *p<0.05, **p<0.01, ***p<0.001.

Jun et al.
Supplementary Fig. 8, Related to Fig. 3



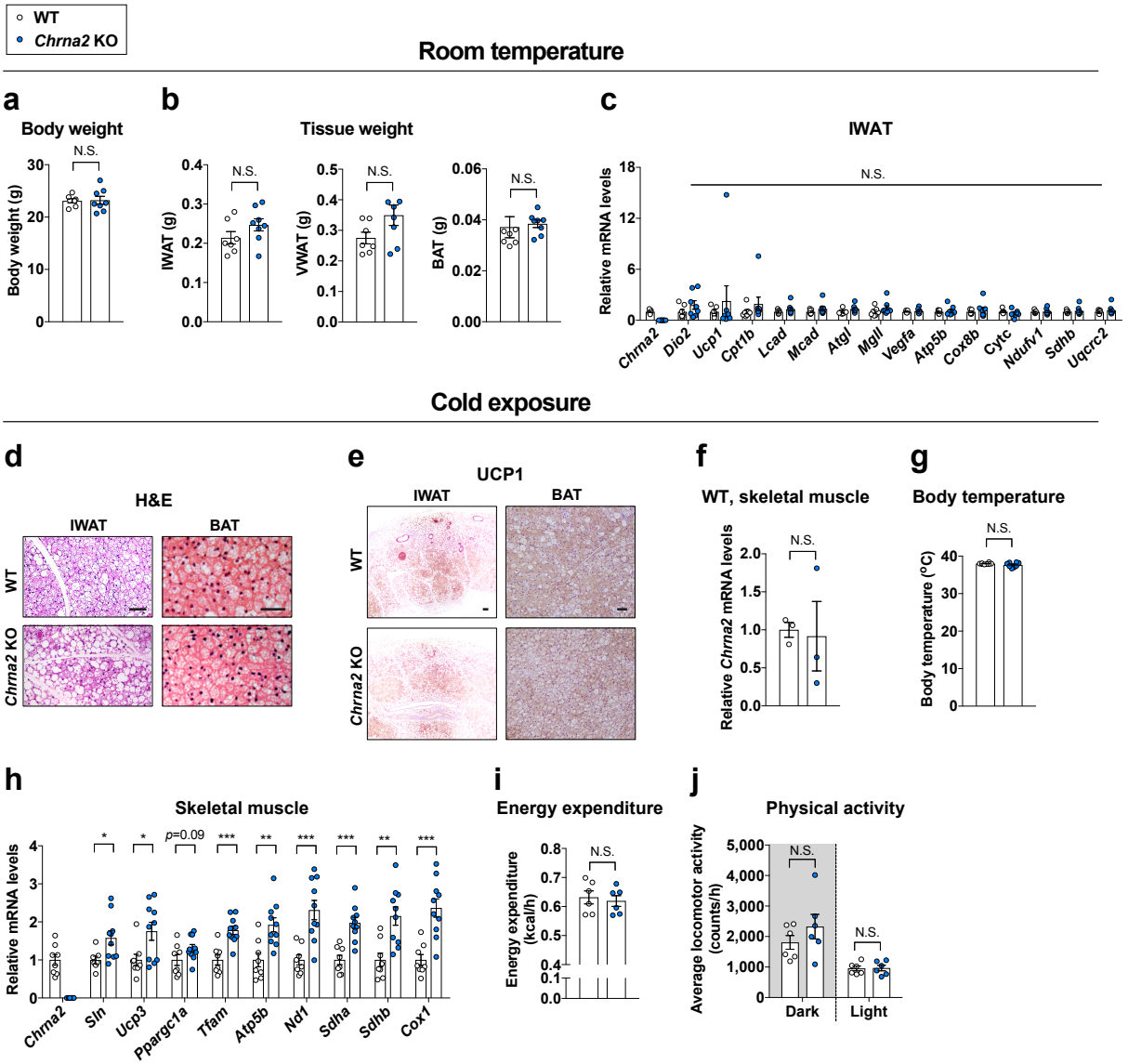
Supplementary Figure 8. Phenotypes of hematopoietic cell-specific ChAT-deleted mice under basal conditions and chronic cold exposure. (**a**) Schematic of the generation of hematopoietic cell-specific *ChAT*-deleted mice. Excision of exons 3 and 4 of the *Chat* gene driven by hematopoietic cell-specific *Vav-iCre* recombinase expression. N and M, 5' noncoding exons. (**b**) qPCR analyses of *Chat* mRNA levels in the spleen (n=5 per group) as a positive control, IWAT (n=15 for fl/fl, 9 for Cre) and interscapular BAT (n=15 for fl/fl, 9 for Cre) of *ChAT*$^{fl/fl}$ and *Vav-iCre*;*ChAT*$^{fl/fl}$ mice. (**c**,**d**) Body (**c**) and fat tissue (**d**) weights of *ChAT*$^{fl/fl}$ and *Vav-iCre*;*ChAT*$^{fl/fl}$ mice housed at room temperature (RT) (n=5 per group). (**e**) Representative images of H&E stained sections of IWAT, VWAT and interscapular BAT from *ChAT*$^{fl/fl}$ and *Vav-iCre*;*ChAT*$^{fl/fl}$ mice housed at RT. Scale bar, 100 μm. (**f**,**g**) qPCR analyses of thermogenic gene expression in IWAT (n=30 for fl/fl, 25 for Cre) (**f**) and interscapular BAT (n=30 for fl/fl, 25 for Cre) (**g**) of *ChAT*$^{fl/fl}$ and *Vav-iCre*;*ChAT*$^{fl/fl}$ mice housed at RT. (**h**) Coculture experiments using inguinal SVF isolated from *ChAT*$^{fl/fl}$ and *Vav-iCre*;*ChAT*$^{fl/fl}$ mice. qPCR analyses of thermogenic markers in differentiated WT inguinal preadipocytes cocultured with or without (Ctrl, n=10) freshly isolated inguinal SVF from *ChAT*$^{fl/fl}$ mice (n=6) and *Vav-iCre*;*ChAT*$^{fl/fl}$ mice (n=10) for 4 h in the presence of rivastigmine (inhibitor of acetylcholinesterase and butyrylcholinesterase) using a two chamber coculture system. (**i**) Changes in body weight of *ChAT*$^{fl/fl}$ and *Vav-iCre*;*ChAT*$^{fl/fl}$ mice following 2 weeks cold exposure (CE) at 10°C (n=5 for fl/fl, 5 for Cre). (**j**) IWAT, VWAT and interscapular BAT fat mass in *ChAT*$^{fl/fl}$ and *Vav-iCre*;*ChAT*$^{fl/fl}$ mice after CE (n=5 for fl/fl, 5 for Cre). (**k**) Rectal body temperature of *ChAT*$^{fl/fl}$ and *Vav-iCre*;*ChAT*$^{fl/fl}$ mice following CE (n=8 per group). (**l**-**o**) qPCR analyses of genes responsible for the adaptive thermogenic response in IWAT (n=14 for fl/fl, 12 for Cre) (**l**,**m**) and BAT (n=9 for fl/fl, 7 for Cre) (**n**,**o**) from *ChAT*$^{fl/fl}$ and *Vav-iCre*;*ChAT*$^{fl/fl}$ mice after CE. (**p**) Model depicting beige-selective signaling via CHRNA2. ChAT-expressing immune cells residing within the inguinal subcutaneous fat depot synthesize acetylcholine, which in turn signals through CHRNA2 and activates the cAMP/PKA pathway to promote beiging. This signaling is beige fat-selective, as acetylcholine-induced calcium uptake only occurs in *Ucp1*-expressing beige fat cells. Data are presented as mean ± s.e.m. **p*<0.05, ****p*<0.001. A different letter denotes a significant difference among groups at *p*<0.05. N.S., not significant.

Jun et al.
Supplementary Fig. 9, Related to Fig. 3



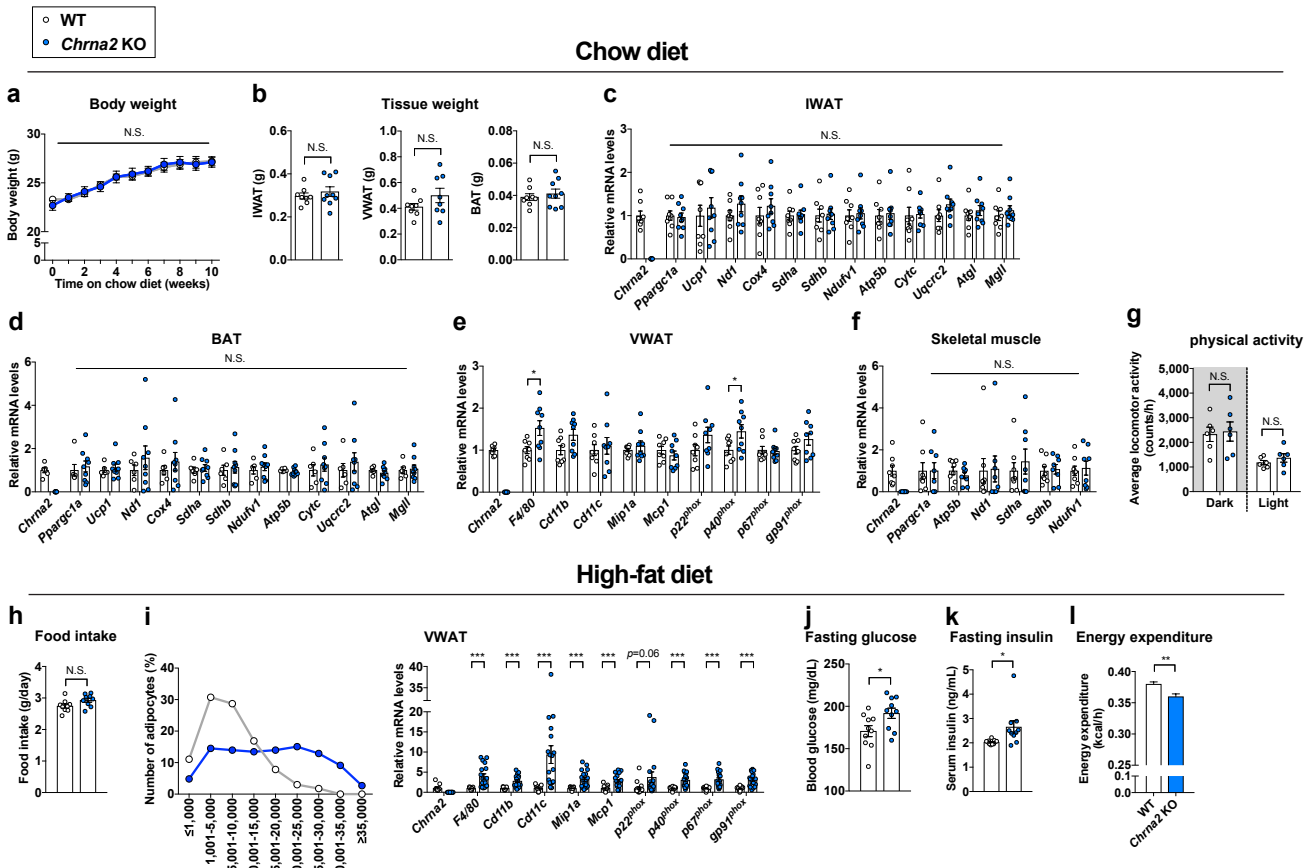
Supplementary Figure 9. *Chrna2* depletion in immune cells has no effects on cold-induced beiging in mouse inguinal fat. (**a**) Experimental outline. Lethally irradiated B6.SJL (B6-CD45.1) recipient mice were transplanted with bone marrow cells (B6-CD45.2) from *Chrna2* KO or littermate WT control mice and then housed at room temperature (RT) or 10°C for 2 d (CE). (**b**) Chimerism analysis in blood cell compartments of WT and *Chrna2* KO bone marrow transplant (BMT) mice through flow cytometric analyses of cells stained for CD45.1 and CD45.2 along with B220, CD19, GR-1, CD11b, TCRβ, CD4, and CD8 (n=15 per group). (**c**) qPCR analyses of thermogenic gene expression in IWAT of WT (n=8 for RT, 7 for CE) and KO (n=7 for RT and CE) BMT mice housed at RT or cold. T cells had a lower turnover rate (about 50-60%) in the chimeras due to the radiation resistance of host memory T cells and some developing thymocytes as previously reported. In addition, KO BMT mice showed a slightly higher replacement of T cells compared to WT BMT mice, however this was not associated with any differences in response to cold between control and KO chimeras. Indeed, mRNA of thermogenic markers, including *Chrna2*, *Ucp1* and *Ppargc1a*, was induced at similar levels in IWAT of both WT and KO BMT mice after cold exposure. Data are presented as mean ± s.e.m. ** $p<0.01$. N.S., not significant. A different letter denotes a significant difference among groups at $p<0.05$.

Jun et al.
Supplementary Fig. 10, Related to Fig. 4



Supplementary Figure 10. Phenotypes of *Chrna2*-deleted mice under basal condition and cold exposure. (**a**) Body weights of WT and *Chrna2* KO mice at room temperature (RT) (n=7 for WT, 8 for KO). (**b**) IWAT, VWAT, and interscapular BAT mass of WT and *Chrna2* KO mice housed at RT (n=7 for WT, 8 for KO). (**c**) qPCR analyses of thermogenic gene expression in IWAT from WT and *Chrna2* KO mice housed at RT (n=7 for WT, 8 for KO). (**d**,**e**) Representative images of H&E staining (**d**) and UCP1 immunohistochemistry (IHC) (**e**) of IWAT and interscapular BAT sections from WT and *Chrna2* KO mice cold exposed at 10°C for 2 weeks. Scale bar, 40 μm. (**f**-**h**) Skeletal muscle shivering compensates the defective inguinal thermogenic capacity in the absence of *Chrna2* under cold exposure. qPCR analyses of *Chrna2* mRNA expression in the skeletal muscle of WT mice housed at room temperature or 10°C for 2 weeks (n=3 per group) (**f**). Rectal body temperature of WT and *Chrna2* KO mice following cold exposure at 10°C for 2 weeks (n=8 per group) (**g**). qPCR analyses of shivering-related genes in the skeletal muscle of WT (n=8) and *Chrna2* KO (n=10) following cold exposure at 10°C for 2 weeks (**h**). (**i**,**j**) Energy expenditure (**i**) and total locomotor activity (**j**) of age- and body weight-matched WT and *Chrna2* KO mice in 12 h light/12 h dark cycle at 5°C (n=6 per group). VO_2 and VCO_2 were collected at 20 min intervals for 23 h from each individual WT and *Chrna2* KO mice with a Comprehensive Lab Animal Monitoring System (Columbus Instruments) and were used to estimate energy expenditure. Total locomotor activity (at x-axis and y-axis) was determined by photo beam sensors while the mice were in indirect calorimetry chambers for measuring energy expenditure. Data are presented as mean ± s.e.m. *p<0.05, **p<0.01, ***p<0.001. N.S., not significant.

Jun et al.
Supplementary Fig. 11, Related to Fig. 5



Supplementary Figure 11. *Chrna2* deficiency causes metabolic abnormalities upon high-fat diet feeding. (**a**) Body weight gain of WT and *Chrna2* KO mice on a chow diet (n=8 for WT, 9 for KO). (**b**) IWAT, BAT and VWAT mass of WT and *Chrna2* KO mice following 10 weeks on a chow diet. (n=8 for WT, 9 for KO). (**c**-**e**) qPCR analyses of thermogenic gene expression in IWAT (n=8 for WT, 9 for KO) (**c**) and BAT (n=6 for WT, 9 for KO) (**d**), and macrophage-related inflammatory gene expression in VWAT (n=8 for WT, 9 for KO) (**e**)) from WT and *Chrna2* KO mice following 10 weeks on a chow diet. (**f**,**g**) qPCR analyses of mitochondrial oxidative phosphorylation-related genes in the skeletal muscle (n=8 per group) (**f**) and locomotor activity in a 12:12 light-dark cycle (n=6 per group) (**g**) of WT and *Chrna2* mice fed a chow diet. (**h**) WT and *Chrna2* KO mice show comparable daily food consumption on a HFD (n=9 per group). (**i**) The ablation of *Chrna2* exacerbates HFD-induced adiposity and inflammation in VWAT. Adipocyte size frequency in VWAT of WT and *Chrna2* KO mice fed on a HFD (left). qPCR analyses of macrophage-related inflammatory gene expression in VWAT of WT and *Chrna2* KO mice fed on a HFD (n=17 for WT, 18 for KO). Chronic inflammation in VWAT plays a crucial role in the development of obesity-related insulin resistance. VWAT of *Chrna2* KO mice fed a HFD demonstrated significantly elevated mRNA levels of macrophage-related inflammatory genes and subunits consisting of NADPH oxidase complex, *p22*^{phox}, *p40*^{phox}, *p67*^{phox} and *gp91*^{phox}, compared to those of control mice (right). (**j**,**k**) *Chrna2* deficiency aggravates the abnormal glucose homeostasis induced by a HFD. Fasting (4 h) blood glucose (n=10 per group) (**j**) and serum insulin (n=11 for WT, 10 for KO) (**k**) levels following a HFD challenge. (**l**) Energy expenditure adjusted to body weight by analysis of covariance (ANCOVA). VO_2 and VCO_2 were collected at 20 min intervals for 48 h from each individual WT and *Chrna2* KO mice fed a HFD for 10 weeks with a Comprehensive Lab Animal Monitoring System (Columbus Instruments) and were used to estimate energy expenditure (n=6 per group). Hourly average energy expenditure for 48 h was calculated and each value (47 values/mouse) was adjusted for body weight using ANCOVA. (**m**,**n**) *Chrna2* deficiency results in minimal effects on skeletal muscle following HFD feeding. qPCR analyses of mitochondrial oxidative phosphorylation-related genes in the skeletal muscle (n=18 for WT, 19 for KO) (**m**) and locomotor activity in a 12 h light/12 h dark cycle (n=8 per group) (**n**) of WT and *Chrna2* KO mice fed a HFD for 10 weeks. Data are presented as mean ± s.e.m. **p*<0.05, ***p*<0.01, ****p*<0.001. N.S, not significant.

Jun et al.
Supplementary Fig. 12

Full-scans of western blots

Figure 2i

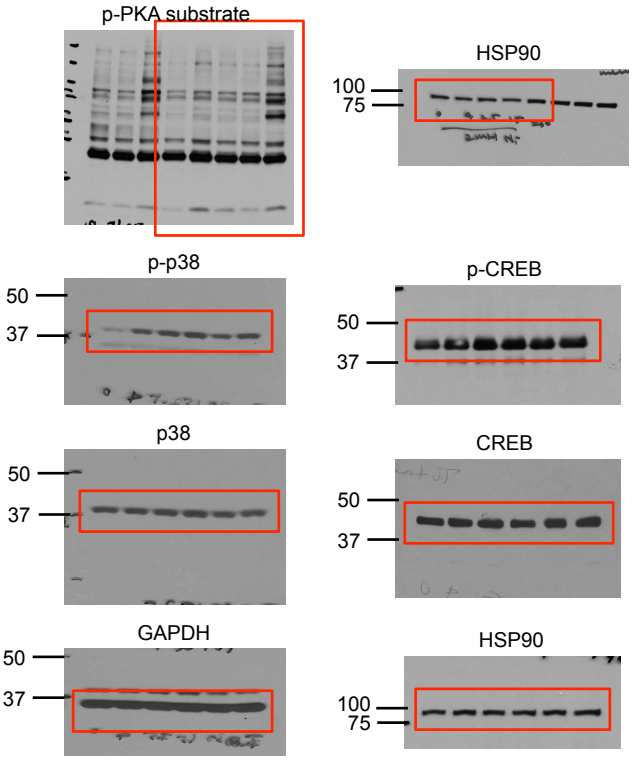
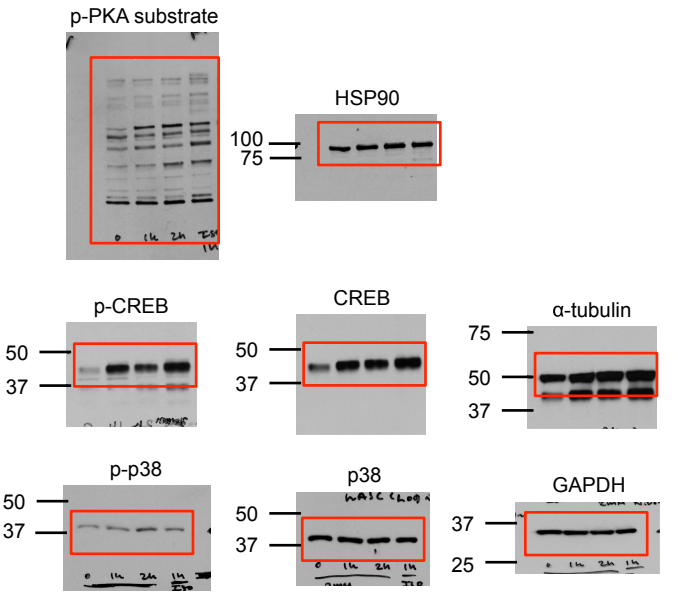


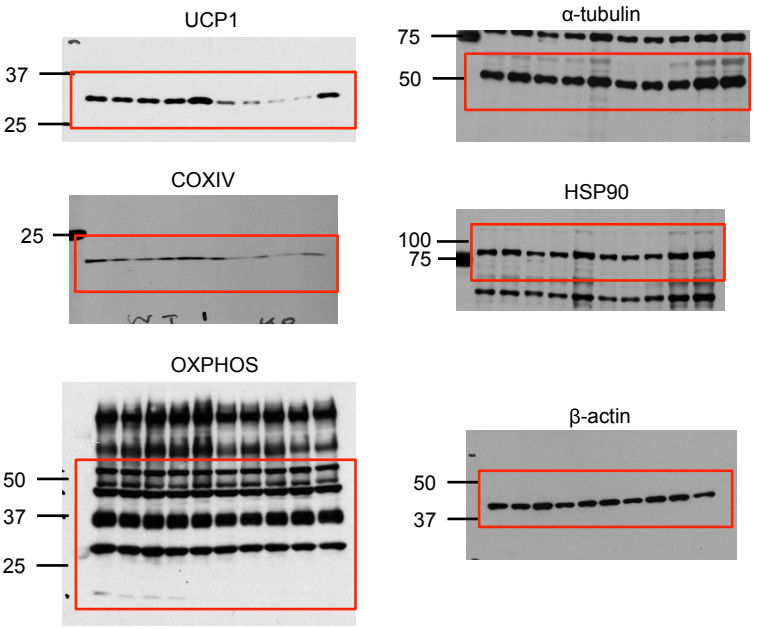
Figure 2j



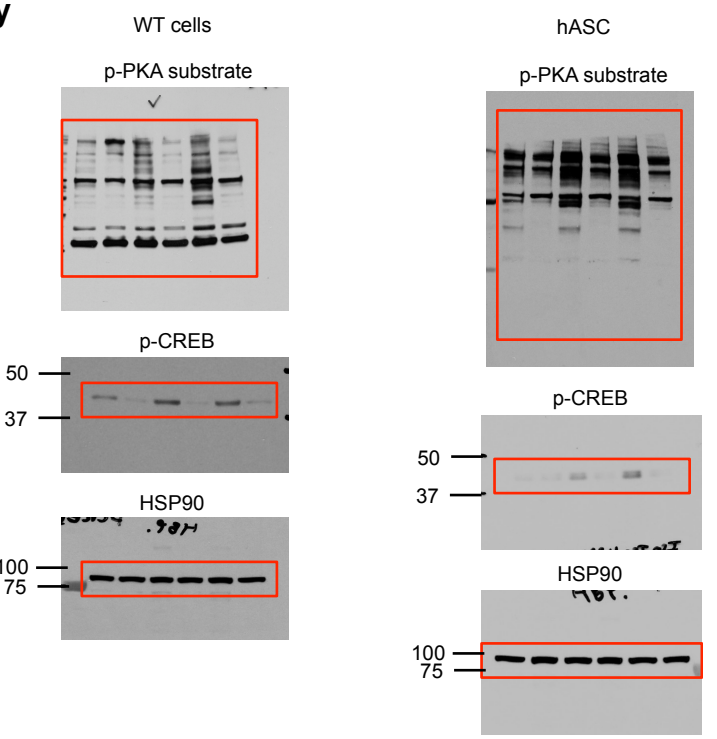
Jun et al.
Supplementary Fig. 12

Full-scans of western blots

Figure 4g



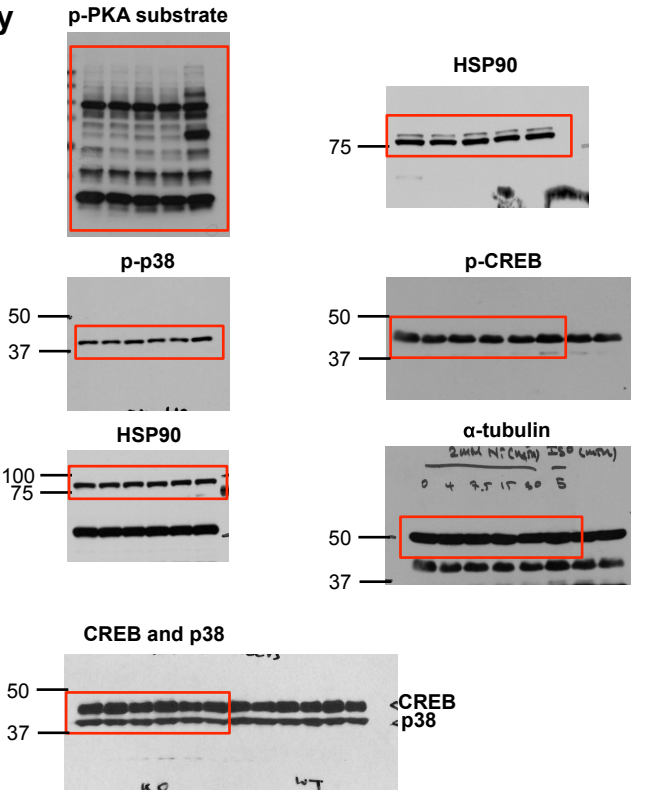
Supplementary Figure 6b



Jun et al.
Supplementary Fig. 12

Full-scans of western blots

Supplementary Figure 6c



Supplementary Table 1. The relative frequencies of immune cell subsets in ChAT-eGFP$^+$ cell population.

Cluster	Subset	Molecular identification scheme	Frequency (%)
i	CD45$^-$ cells		1.3±0.2
	CD45$^+$ cells		98.7±0.2
ii	MΦ1	CD45$^+$/F4/80$^+$/CD11b$^+$/MHC Class II$^+$/CD11c^{high}/CD206$^-$	3.3±0.1
iii	MΦ2	CD45$^+$/F4/80$^+$/CD11b$^+$/MHC Class II$^+$/CD11c^{med}/CD206$^+$	8.5±0.4
iv	DN MΦ	CD45$^+$/F4/80$^+$/CD11b$^+$/MHC Class II$^+$/CD11c$^-$/CD206$^-$	3.0±0.1
v	γδT cell	CD45$^+$/F4/80$^-$/CD11b$^-$/CD3$^+$/TCRγδ$^+$	5.4±1.5
vi	CD4$^+$ αβT cell	CD45$^+$/F4/80$^-$/CD11b$^-$/CD3$^+$/TCRβ$^+$/CD4$^+$	15.6±1.1
vii	CD8$^+$ αβT cell	CD45$^+$/F4/80$^-$/CD11b$^-$/CD3$^+$/TCRβ$^+$/CD8$^+$	0.7±0.0
viii	CD4$^-$CD8$^-$ αβT cell	CD45$^+$/F4/80$^-$/CD11b$^-$/CD3$^+$/TCRβ$^+$/CD4$^-$/CD8$^-$	4.3±0.1
ix	B220$^+$ B cell	CD45$^+$/F4/80$^-$/CD11b$^-$/CD19$^+$/B220$^+$	44.5±2.5
x	B220$^-$ B cell	CD45$^+$/F4/80$^-$/CD11b$^-$/CD19$^+$/B220$^-$	4.7±0.2
	Eosinophil	CD45$^+$/F4/80$^+$/CD11b$^+$/Siglec-F$^+$	0.0±0.0*
	Others	Others	8.6±1.2

*There were almost no ChAT-eGFP$^+$ cells that expressed the eosinophil marker Siglec-F.

Supplementary Table 2. Primer sequences for PCR analysis

Gene	Full name	5′ Primer	3′ Primer
qPCR			
Mouse			
Atgl (Pnpla2)	Patatin-like phospholipase domain containing 2	AACACCAGCATCCAGTTCAA	GGTTCAGTAGGCCATTCCTC
Atp5b	ATP synthase, H+ transporting mitochondrial F1 complex, beta subunit	GGTTCATCCTGCCAGAGACTA	AATCCCTCATCGAACTGGACG
Cd11b (Itgam)	Integrin alpha M	AAACCACAGTCCCGCAGAGA	CGTGTTCACCAGCTGGCTTA
Cd11c (Itgax)	Integrin alpha X	ACACAGTGTGCTCCAGTATGA	GCCCAGGGATATGTTCACAGC
Cd45 (Ptprc)	Protein tyrosine phosphatase, receptor type, C	GAACATGCTGCCAATGGTTCT	TGTCCCACATGACTCCTTTCC
Chat	Choline acetyltransferase	TGCCAGTCAACTCTAGCCCT	CTGCAAACCTTAGCTGGTCATT
Chrna1	Cholinergic receptor, nicotinic, alpha polypeptide 1 (muscle)	ACCAATGTACGTCTGAAACAGC	TTTTCCGAGGGGATGTGAATTTT
Chrna2	Cholinergic receptor, nicotinic, alpha polypeptide 2 (neuronal)	GCCACCGGAACCTATAACAGC	CCGGCGGATAACGAAGTAGTA
Chrna3	Cholinergic receptor, nicotinic, alpha polypeptide 3	TGGAAACCCTCTGACTACCAA	GGCGTTGTTGTAAAGCACGA
Chrna4	Cholinergic receptor, nicotinic, alpha polypeptide 4	CTGTCGCAATGAACACCATCT	ATGGCGAACTTCACACCTGTC
Chrna5	Cholinergic receptor, nicotinic, alpha polypeptide 5	GTTGCCTGAGCTATCCTCTGC	GACGAACCCACTTTTCATAGTCT
Chrna6	Cholinergic receptor, nicotinic, alpha polypeptide 6	TTGCTCACTACAACCGCTTCA	GCGTGATTGCCAATTCAAAATGC
Chrna7	Cholinergic receptor, nicotinic, alpha polypeptide 7	AGTTTTAACCACCAACATTTGGC	TTTTCACTCCGGGGTACTCAG
Chrna9	Cholinergic receptor, nicotinic, alpha polypeptide 9	CAGGTCACGCTCTCCCAGATA	GTACGCATCGTGCCAAGTTT
Chrna10	Cholinergic receptor, nicotinic, alpha polypeptide 3	ATGGATGAACGGAACCAAGTG	GTCCCAATGTAGGTAGGCGT
Chrnb1	Cholinergic receptor, nicotinic, beta polypeptide 1 (muscle)	ACTACAGGTTAAGCTGGGACC	GTCCAGGGCAACGTCGAAAT
Chrnb2	Cholinergic receptor, nicotinic, beta polypeptide 2	AGGGGTTTTGGGTACTGACAC	GGATCAGCTTGTTATAGCGGGAA
Chrnb3	Cholinergic receptor, nicotinic, beta polypeptide 3	TGCTGACGGACGTTTTGAGG	GAGGAGTCCAACTGACGGT
Chrnb4	Cholinergic receptor, nicotinic, beta polypeptide 4	GCTATGTGGACGTGACCTATG	CGACGTGATGAGCACACAAG
Cox1	Cytochrome c oxidase subunit I	CTACTATTCGGAGCCTGAGC	GCATGGGCAGTTACGATAAC
Cox4	Cytochrome c oxidase subunit IV isoform 1	ACCAAGCGAATGCTGGACAT	GGCGGAGAAGCCCTGAA
Cox8b	Cytochrome c oxidase subunit VIIIb	GAACCATGAAGCCAACGACT	GCGAAGTTCACAGTGGTTCC
Cpt1b	Carnitine palmitoyltransferase 1b	ATCATGTATCGCCGCAAACT	CCATCTGGTAGGAGCACATGG
Cytc (Uqcrfs1)	Ubiquinol-cytochrome c reductase, Rieske iron-sulfur polypeptide 1	ACAAGAAGACTCAAATGTGTTTCAGT	TGCACTGTCAAGAATAGACAGTTG
Dio2	Deiodinase, iodothyronine, type II	CATCTTCCTCCTAGATGCCTA	CTGATTCAGGATTGGAGACGTG
F4/80 (Adgre1)	Adhesion G protein-coupled receptor E1	CCCCAGTGTCCTTACAGAGTG	GTGCCCAGAGTGGATGTCT
Gfp	Green fluorescent protein	GCGGATCTTGAAGTTCACCTTGAT	CACGACTTCTTCAAGTCCGCCATG
gp91^{phox} (Cybb)	Cytochrome b-245, beta polypeptide	TTGGGTCAGCACTGGCTCTG	TGGCGGTGTGCAGTGCTATC
Hsl	Lipase, hormone-sensitive	TGAGATGCCACTCACCTCTG	GCCTAGTGCCTTCTGGTCTG
Nd1	NADH dehydrogenase subunit 1	GGGATAACAGCGCAATCCTA	ATCGTTGAACAAACGAACCA
Lcad (Acadl)	Acyl-Coenzyme A dehydrogenase, long-chain	TCTTTTCCTCGGAGCATGACA	GACCTCTCTACTCACTTCTCCAG
Mcad (Acadm)	Acyl-Coenzyme A dehydrogenase, medium chain	AGGGTTTAGTTTTGAGTTGACGG	CCCCGCTTTTGTCATATTCCG
Mcp1 (Ccl2)	Chemokine (C-C motif) ligand 2	TTAAAAACCTGGATCGGAACCAA	GCATTAGCTTCAGATTTACGGGT
Mgll	Monoglyceride lipase	TGATTTCACCTCTGGTCCTTG	GTCAACCTCCGACTTGTTCC
Mip1a (Ccl3)	Chemokine (C-C motif) ligand 3	TTCTCTGTACCATGACACTCTGC	CGTGGAATCTTCCGGCTGTAG
Ndufv1	NADH dehydrogenase (ubiquinone) flavoprotein 1	TTTCTCGGCGGGTTGGTTC	GGTTGGTAAAGATCCGGTCTTC
p22^{phox} (Cyba)	Cytochrome b-245, alpha polypeptide	GTCCACCATGGAGCGATGTG	CAATGGCCAAGCAGACGGTC
p40^{phox} (Ncf4)	Neutrophil cytosolic factor 4	GCCGCTATCGCCAGTTCTAC	GCAGGCTCAGGAGGTTCTTC
p67^{phox} (Ncf2)	Neutrophil cytosolic factor 2	CTGGCTGAGGCCATCAGACT	AGGCCACTGCAGAGTGCTTG
Pparg	Peroxisome proliferator-activated receptor gamma	GCATGGTGCCTTCGCTGA	TGGCATCTCTGTGTCAACCATG
Ppargc1a	Peroxisome proliferator-activated receptor gamma, coactivator 1 alpha	AGCCGTGACCACTGACAACGAG	GCTGCATGGTTCTGAGTGCTAAG
Sdha	Succinate dehydrogenase complex, subunit A, flavoprotein (Fp)	GGAACACTCCAAAAACAGACCT	CCACCACTGGGTATTGAGTAGAA
Sdhb	Succinate dehydrogenase complex, subunit B, iron sulfur (Ip)	AATTTGCCATTTACCGATGGGA	AGCATCCAACACCATAGGTCC
Sln	Sarcolipin	TGAGGGGCCATGCTATACTC	GCATTGTGAGTGTGGGTCAG
Tbp	TATA box binding protein	GAAGCTGCGGTACAATTCCAG	CCCCTTGTACCCTTCACCAAT
Td-tomato	Tandem-dimer tomato	GCGTTACATAACTTACGGTAAATGGCCC	GGGCGTACTTGGCATATGATACACTTGATG
Tfam	Transcription factor A, mitochondrial	ATTCCGAAGTGTTTTTCCAGCA	TCTGAAAGTTTTGCATCTGGGT
Ucp1	Uncoupling protein 1	ACTGCCACACCTCCAGTCATT	CTTTGCCTCACTCAGGATTGG
Ucp3	Uncoupling protein 3	GGATTTGTGCCCTCCTTTCTG	AGATTCCCGCAGTACCTGGACT
Uqcrc2	Ubiquinol cytochrome c reductase core protein 2	AAAGTTGCCCCGAAGGTTAAA	GAGCATAGTTTTCCAGAGAAGCA
Vegfa	Vascular endothelial growth factor A	GCACATAGAGAGAATGAGCTTCC	CTCCGCTCTGAACAAGGCT
Human			
CHRNA2	Cholinergic receptor, nicotinic, alpha polypeptide 2 (neuronal)	AGGCTCGCATACCGAGACT	TCACCACGTCTGAAGTGTTGG
TBP	TATA box binding protein	CCACTCACAGACTCTCACAAC	CTGCGGTACAATCCCAGAACT
UCP1	Uncoupling protein 1	AGGTCCAAGGTGAATGCCC	GCGGTGATTGTTCCCAGGA
Mitochondrial DNA			
nuc*Rip140*	Receptor-interacting protein 140, nuclear	TCCCCGACACGAAAAAGAAAG	ACATCCATTCAAAAGCCCAGG
mt*Cox1*	Cytochrome c oxidase I, mitochondrial	CTACTATTCGGAGCCTGAGC	GCATGGGCAGTTACGATAAC
ChIP, conventional PCR			
Chrna2 pro.	*Chrna2* promoter	GCTTTTCCACCAAACACACC	CAAGCGTGACTTTGAGTCCA
Neg. Ctrl.	Negative control	CCTTGCCCTGTGGTCTAATC	CTGACAGATGGCACTCCAGA